Effect of Seepage-Induced Nonhydrostatic Pressure Distribution on Bed-Load Transport and Bed Morphodynamics

Simona Francalanci[1]; Gary Parker[2]; and Luca Solari[3]

Abstract: Bed-load transport is commonly evaluated in the condition of a hydrostatic pressure distribution of the flow field; while this condition is reasonable for quasi-steady, quasi-uniform rectilinear flows, it cannot be satisfied in a large variety of flow conditions, i.e., near an obstacle as in the case of a bridge pier. The dimensionless Shields number, which contains the assumption of a hydrostatic pressure distribution in its denominator, therefore cannot be strictly applied to evaluate bed-load transport in all the configurations where nonhydrostatic pressure distributions are observed. In the present work, a generalization of the Shields number is proposed for the case of nonhydrostatic pressure distribution produced by groundwater flow. Experiments showing the effects of vertical groundwater flow on the bed morphodynamics are presented. The comparison between the experimental observations and numerical results, obtained by means of a morphodynamic model which employs the new formulation of the Shields number, suggests that the proposed generalization of the Shields number is able to account the effect of the nonhydrostatic pressure distribution on the bed-load transport.

CE Database subject headings: Hydrostatic pressure; Sediment transport; Seepage; Shear stress; Bed load.

Introduction

Fluvial sediment mobility has been traditionally expressed in terms of the dimensionless Shields number τ_*, defined as follows, where τ_b=boundary shear stress; g=gravitational acceleration; D=characteristic grain size of sediment at the bed surface; ρ=density of water; and ρ_s=density of sediment

$$\tau_* = \frac{\tau_b}{(\rho_s - \rho)gD} \quad (1)$$

The Shields number specifically scales the ratio of the impelling drag force of the water acting on a grain at the bed surface (numerator) to the Coulomb force that resists motion, which can be taken to be proportional to the immersed weight of the grain (denominator). This can be seen more clearly by rewriting Eq. (1) in the form

[1]Postdoctoral Researcher, CERAFRI, Center of Research and Advanced Education for Hydrogeological RIsk Prevention, Via XI Febbraio 2, Retignano di Stazzema (LU), Italy. E-mail: simona.francalanci@dicea.unifi.it

[2]Professor, Ven Te Chow Hydrosystems Laboratory, Univ. of Illinois, 205 N. Mathews Ave., Urbana, IL 61801. E-mail: parkerg@uiuc.edu

[3]Researcher, Dept. of Civil and Environmental Engineering, Univ. degli Studi di Firenze, Via S. Marta 3, 50139 Firenze, Italy (corresponding author). E-mail: luca.solari@dicea.unifi.it

$$\tau_* = \frac{\tau_b \frac{1}{2}\pi\left(\frac{D}{2}\right)^2}{\frac{4}{3}(\rho_s - \rho)g\frac{4}{3}\pi\left(\frac{D}{2}\right)^3} \quad (2)$$

The threshold of motion has been defined in terms of a critical Shields number τ_{*cr} (Shields 1936), and appropriately defined dimensionless measures of the magnitude of sediment transport have been taken to be functions of the Shields number [e.g., the version of the bed-load transport relation of Meyer-Peter and Müller (1948) specified by Chien (1954)]. In more recent years the concept of the Shields number has been extended to encompass a vectorial boundary shear stress vector that may act in an arbitrary direction within the plane of the bed (e.g., Seminara et al. 2002; Parker et al. 2003; Francalanci 2006; Francalanci and Solari 2007).

It does not seem to be generally recognized, however, that by its very definition the Shields number assumes the pressure distribution of the water in which sediment grains are immersed to be hydrostatic. Consider, for example, a spherical grain of diameter D. The origin of the term $(\rho_s-\rho)$ in Eqs. (1) and (2) is the assumption that the downward gravitational force F_g corresponding to the weight of an immersed particle, given as

$$F_g = \rho_s g \frac{4}{3}\pi\left(\frac{D}{2}\right)^3 \quad (3)$$

is partially counterbalanced by the upward Archimedian buoyant pressure force F_p corresponding to the weight of the displaced fluid, given as

$$F_p = \rho g \frac{4}{3}\pi\left(\frac{D}{2}\right)^3 \quad (4)$$

so that the effective gravitational force F_g' of the particle is given as

$$F'_g = F_g - F_p = (\rho_s - \rho) g \frac{4}{3} \pi \left(\frac{D}{2} \right)^3 \tag{5}$$

The above term specifically appears in the denominator of Eq. (2).

The form of the buoyant pressure force given by Eq. (4) is obtained from the assumption of a hydrostatic pressure distribution, i.e., one such that pressure p satisfies the relation

$$\frac{\partial p}{\partial x_i} = -\rho g \delta_{i3} = -\rho g (0,0,1) \tag{6}$$

where x_i denotes position vector in index notation; $x_3 = z$ denotes upward vertical coordinate; and δ_{ij} denotes Kronecker delta. The vectorial pressure force F_{pi} acting on an immersed grain is given as

$$F_{pi} = -\int\int p|_{\text{surface}} n_{oi} dS \tag{7}$$

where the pressure is evaluated at the surface of the particle; n_{oi} = outward normal unit vector to the surface; and dS = element of surface area. Reducing Eq. (7) with the divergence theorem and evaluating the result under the assumption of hydrostatic pressure according to Eq. (6), it is found that

$$F_{pi} = -\int\int\int \frac{\partial p}{\partial x_i} dV = \left[0,0,\rho g \frac{4}{3} \pi \left(\frac{D}{2} \right)^3 \right] \tag{8}$$

i.e., the vectorial generalization of Eq. (4).

The assumption of hydrostatic pressure is an accurate one for the case of nearly steady, relatively uniform rectilinear flow. In the case of flow around an obstacle such as a bridge pier, however, nonhydrostatic pressure forces can be significant. If the Shields number does indeed represent an appropriate nondimensional ratio characterizing sediment transport, the concept should somehow generalize to nonhydrostatic pressure distributions.

The net force acting on a bed particle due to a nonhydrostatic pressure distribution can in principle act in any direction. Here, however, for simplicity the problem is restricted to pressure variation solely in the vertical, so that

$$\frac{\partial p}{\partial x_1} = \frac{\partial p}{\partial x_2} = 0 \tag{9}$$

A dimensionless number $\mathbf{Nh}$ characterizing deviation from hydrostatic conditions can then be defined as

$$\mathbf{Nh} = -\frac{1}{\rho g} \frac{\partial p}{\partial x_3} \tag{10}$$

An extension of Eq. (8) using Eq. (10) leads to the following relation for the pressure force on an immersed bed particle

$$F_{pi} = \left[0,0,\rho g \frac{4}{3} \pi \left(\frac{D}{2} \right)^3 \mathbf{Nh} \right] \tag{11}$$

where $\mathbf{Nh}$ is evaluated at the sediment bed. Thus a vertical pressure gradient that is stronger than hydrostatic in the vertical ($\partial p / \partial z < -\rho g$ and $\mathbf{Nh} > 1$) in the vicinity of a grain on the bed leads to an enhanced buoyant force on the grain, and a vertical pressure gradient that is weaker than hydrostatic ($\partial p / \partial z > -\rho g$ and $\mathbf{Nh} < 1$) in the vertical leads to a reduced buoyant force on the grain. The former case ought to make a grain effectively lighter and thus more mobile, and the latter case should make the same grain effectively heavier and thus less mobile, as illustrated in Fig. 1.
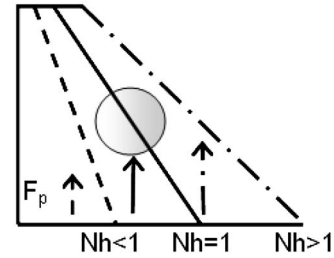

Fig. 1. Vertical pressure gradient dp/dz near bed and buoyant force F_p acting on bed particle

The appropriate generalization of the Shields number that correctly characterizes the pressure force for this case is

$$\tau_* = \frac{\tau_b}{(\rho_s - \rho \mathbf{Nh}) g D} \tag{12}$$

As expected, a value of $\mathbf{Nh}$ that is somewhat greater than 1, for example, reduces the denominator, and thus increases τ_* and hence the mobility of a grain on the bed. If the concept of the Shields number itself is correct, a correlation between dimensionless sediment transport rate and Shields number that works for a hydrostatic pressure distribution should also work for the nonhydrostatic pressure distribution hypothesized here, with the simple generalization of the Shields number from Eqs. (1)–(12). This paper is devoted to the testing of this hypothesis.

Vertical Seepage as Means of Generating Nonhydrostatic Pressure Distribution

Cheng and Chiew (1999) considered the case of upward seepage flow in a granular, erodible bed under an open channel flow. They found that such a seepage flow reduces the critical shear velocity for the onset of motion of the bed sediment at the surface. Their method was adapted to the present work to create a nonhydrostatic pressure distribution within the pore water of the sediment bed.

Here a seepage, or groundwater flow, is allowed only in the vertical direction. The piezometric head h_p is given as

$$h_p = \frac{p}{\rho g} + z \tag{13}$$

The vertical velocity of seepage v_s is related to h_p according to Darcy's law

$$v_s = -K \frac{dh_p}{dz} = -K \left(1 + \frac{1}{\rho g} \frac{dp}{dz} \right) \tag{14}$$

where K denotes the hydraulic conductivity of the granular bed. Between Eqs. (10), (12), and (14) it is readily seen that
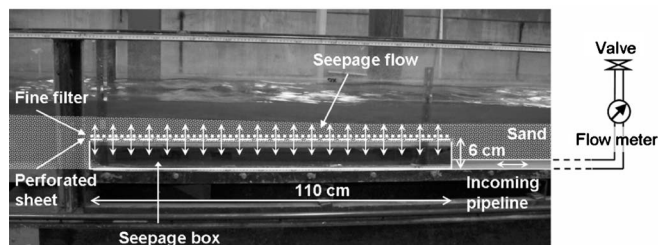
$$\mathbf{Nh} = -\frac{1}{\rho g} \frac{dp}{dz} = 1 + \frac{v_s}{K} \tag{15}$$

$$\tau_* = \frac{\tau_b}{\left[\rho_s - \rho \left(1 + \frac{v_s}{K} \right) \right] g D} \tag{16}$$

An upward seepage thus causes a nonhydrostatic pressure distribution with $\mathbf{Nh} > 1$, and thus enhanced particle mobility according to Eq. (16), and a downward seepage has the opposite effect.
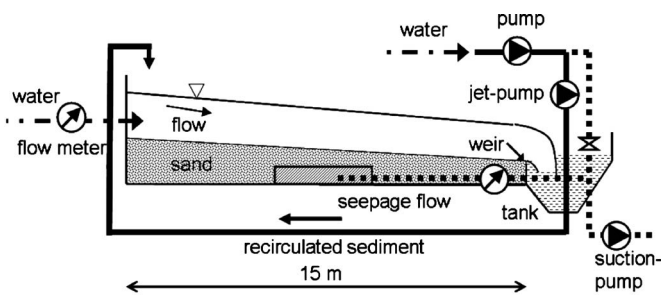
(a)

(b)

Fig. 2. Experimental setup: (a) sketch of the experimental apparatus; (b) sketch of the seepage box

Table 1. Hydraulic Conditions for the Experiments; Run Codes $1 \div 5$ Pertain to Runs with Upward Groundwater Flow, and Run Codes $4 \div 6$ Pertain to Runs with Downward Groundwater Flow.

Run Code	Q_w (L/s)	Q_{seepage} (L/min)
1	20.6	20, 40. 60, 80, 100, 140
2	16	20, 40. 60, 80, 100, 140
3	12	20, 40. 60, 80, 100, 140
4	20.6	30, 60, 90
5	16	30, 60, 90
6	12	30, 60, 90

These tendencies are summarized in Fig. 1. As noted below, the cases studied here include both upward and downward seepage.

Experimental Setup and Protocol

Experiments were carried out in a glass-sided sediment-recirculating, water-feed flume that was 15 m long, 0.61 m wide, and 0.4 m deep. The incoming water discharge was controlled by a valve and monitored with an electromagnetic flow meter. The bed of the flume was covered with sediment. Nearly all the water overflowed from a collecting tank at the downstream end of the flume and exited the system. The sediment settled to the bottom of the collecting tank, and was recirculated with a jet-pump system to the upstream end of the flume with a small discharge of water as a slurry, where it was reintroduced. A sketch of the flume is provided in Fig. 2(a).

Upward or downward groundwater flow was introduced in a reach between 9 and 10.1 m downstream of the upstream end of the flume. The seepage flow passed through a seepage box buried underneath the flume bed. The seepage box had a length of 1.1 m, a width of 0.61 m, and a height of 0.06 m. A perforated sheet over the top of the box regulated the seepage flow, which was verified to be nearly uniform over the length of the reach and width of the flume. A fine filter was inserted above the perforated sheet in order to separate the sand layer from the water inside the box. In the case of upward seepage, water was delivered by a second jet pump into a seepage box through a pipeline. The groundwater flow discharge to the seepage box was regulated by a valve and measured by an electromagnetic flow meter. In the case of downward seepage the water was extracted from the seepage box by a suction pump. A sketch of the configuration for the seepage box is given in Fig. 2(b). The employed setup was designed to realize a uniform seepage flow that was directed as nearly normal to the bed as possible; as a result seepage velocity is here assumed to have had a negligible component tangential to the bed.

A relatively uniform sediment was chosen for the experiments

in order to minimize sorting effects. The characteristic size was chosen such that the effect of bed forms was not too large. In addition, trial experiments with a variety of sediment sizes showed that uniform groundwater flow could not be maintained when the sediment was too fine, and that the seepage discharge could not be controlled accurately when the sediment was too coarse. These trial experiments allowed the selection of a sediment with a value of hydraulic conductivity K that was appropriate for the experiments.

The sediment selected for the experiments was subject to some initial sorting, because the finest material in the mix was gradually washed out of the collection box. After some time, however, the sediment in the flume equilibrated to a median size D_{50} and geometric mean size D_g both near 0.84 mm, a size D_{35} near 0.69 mm, a size D_{90} near 1.48 mm, and a geometric standard deviation σ_g near 1.62. Hydraulic conductivity K was measured with a Darcy tube and found to be near 0.0025 m/s.

Velocity measurements were performed using a micropropeller with a diameter of 14 mm. A point gauge was used to measure water surface elevations and the elevation of the bed. Five bed elevation points were measured for each transverse cross section; the average of these values was assumed to be the cross-sectional mean value of the bottom elevation for the purpose of characterizing long profiles. Measurements of sediment transport in the flume were obtained by diverting slurry from the sediment recirculation pipe and measuring the sediment mass collected as a function of time.

The experimental protocol was designed around Table 1. The table encompasses inflow discharges Q_w ranging from 12 to 20.6 L/s, upward seepage discharges Q_{seepage} ranging from 20 to 140 L/min, and downward seepage discharges Q_{seepage} ranging from 30 to 90 L/min, for a total of 27 experimental conditions, 18 of which pertained to upward seepage and 9 of which pertained to downward seepage. In principle, each experimental condition corresponded to a set of three experiments: one with no seepage, one with data acquired after 10 min of seepage (short-term experiment), and one with data acquired after 2 or 4 h of seepage (the longer time span corresponding to lower seepage rates). Run 2-2, for example, corresponds to the second-highest seepage rate for Run Code 2 in Table 1, for which $Q_w=16$ L/s and $Q_{\text{seepage}}=40$ L/min.

The first experiment in each set of three was conducted with the specified value of inflow discharge Q_w but in the absence of seepage. Each such experiment was continued until mobile-bed equilibrium was obtained; the results provided baseline data on sediment transport and flow resistance. In some cases a run was repeated in order to test for consistency. As a consequence, results for 33 experiments without seepage are reported here.

For the second experiment of each set of three, the flow was

Fig. 3. Bed forms at equilibrium configuration without seepage

restarted, but this time with the introduction of seepage over the 1.1 m reach specified in Fig. 2(a). The bed elevation was allowed to evolve due to the effect of the seepage flow, and the flow was stopped after 10 min to measure the bed profile. These experiments are referred to as "short-term experiments." For the third experiment of each set, the flow was restarted and then continued for a total of 2 h (higher seepage rate) or 4 h (lower seepage rate), after which data were acquired. Both durations include 10 min of the short-term experiment. These experiments are referred to as "long-term experiments." Long-term experiments were not performed, however, for cases with a seepage discharge Q_{seepage} of 140 L/min. In several cases short-term and long-term experiments were repeated, in order to confirm the experimental data. In the case of repeated runs, the values for the data reported here were typically obtained by averaging the data from the repeat experiments. In a very small number of cases of long-term experiments, the duration differed between the repeat experiments (2 h versus 4 h); in such cases the data are reported separately.

Mobile-Bed Equilibrium in Absence of Seepage

A total of 33 experiments were first performed so as to obtain mobile-bed equilibrium conditions in the absence of seepage. These experiments were performed with flow discharges Q_w ranging from 12.0 to 20.6 L/s (Table 1). Each experiment was continued for a minimum of 12 h in order to ensure that mobile-bed equilibrium was attained. In all cases sediment was observed to move exclusively as bed-load transport. The bed forms that covered the bed at mobile-bed equilibrium can be seen in Fig. 3.

In the absence of sediment loss from the collection box at the downstream end of the flume, the total mass of sediment is conserved in a sediment-recirculating flume. In the flume used for the experiments the downstream elevation of the bed was held constant by an overflow wall, comprised of a wooden submerged weir, spanning the whole cross section, with its top leveled with the downstream bed elevation. The combination of these two conditions requires that the bed slope at mobile-bed equilibrium be constant for a given mass of sediment in the flume, and that this same bed slope must increase linearly with increasing mass of sediment in the flume. While the total amount of sediment in the flume was varied somewhat from run to run, the equilibrium bed slope S varied within a relatively narrow range for the 33 experi-

ments without seepage, with 79% of the experiments showing a value of S within $\pm 10\%$ of a value of 0.00384.

The results of the measurements at mobile-bed equilibrium allowed the characterization of hydraulic resistance and bed-load transport. Part of the drag force of the flow in the flume is expended against the nonerodible vertical sidewalls of the flume, and thus does not contribute to sediment transport. The part of the drag force expended against the erodible bed of the flume can be further decomposed into form drag associated with the bed forms and skin friction; only the latter is effective in moving sediment in bed-load transport. The total boundary shear stress on the bed τ_b is here characterized in terms of the corresponding total bed shear velocity u_*, where

$$u_* = \sqrt{\frac{\tau_b}{\rho}} \qquad (17)$$

The total bed shear velocity was estimated from the following relation appropriate for steady, uniform flow

$$u_* = \sqrt{gRS} \qquad (18)$$

where R=hydraulic radius of the bed region (as opposed to the sidewall region), here estimated from the relation

$$R = \begin{cases} \dfrac{B}{4} & \text{for } H > B/2 \\ \dfrac{1}{B}[H^2 + H(B - 2H)] & \text{for } H < B/2 \end{cases} \qquad (19)$$

of Vanoni and Brooks (1957); in the above relation B=channel width; and H=flow depth. The hydraulic radius R' associated with skin friction only was obtained by means of a trial-and-error procedure based on the calculation of the corresponding skin friction shear velocity u_*'. The latter quantity was estimated using the relation for dimensionless Chézy coefficient C' due to Parker (1991), i.e.

$$u_*' = \frac{U_{\text{measured}}}{C'} = \frac{U_{\text{measured}}}{8.1 \cdot \left(\dfrac{R'}{2D_{90}}\right)^{1/6}} \qquad (20)$$

where U_{measured} denotes cross-sectionally averaged flow velocity as determined from measurements with a propeller meter. With the calculated value of u_*', R' is obtained with a modified version relation Eq. (18) in which only skin quantities related to skin friction are specified. The procedure is repeated iteratively until convergence is reached.

The Shields number associated with total bed friction τ_* and the corresponding Shields number τ_*' associated with skin friction only were then computed as
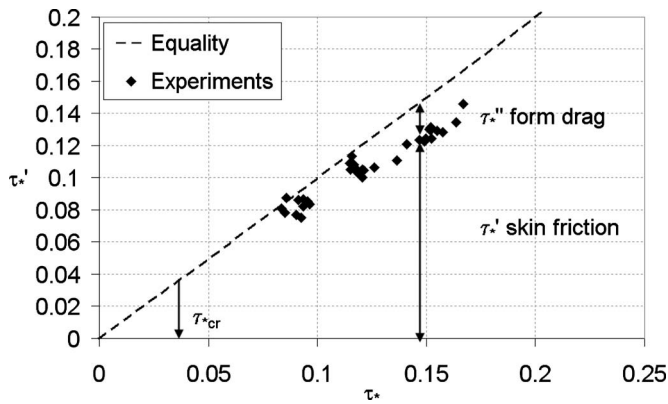
$$\tau_* = \frac{\rho u_*^2}{(\rho_s - \rho)gD_{50}} \qquad (21a)$$

$$\tau_*' = \frac{\rho u_*'^2}{(\rho_s - \rho)gD_{50}} \qquad (21b)$$

A plot of τ_*' versus τ_* is given in Fig. 4; the Shields number due to form drag τ_*'' indicated in the figure is given as

$$\tau_*'' = \tau_* - \tau_*' \qquad (22)$$

The critical Shields number $\tau_{*\text{cr}}$ for the onset of sediment motion was estimated to be equal to 0.0332, in accordance with the criteria of Shields (1936).

Fig. 4. Decomposition of total dimensionless bed-shear stress into component due to skin friction and component due to form drag. Data are for experiments reported here.

The bed-load transport rates observed in the 33 experiments pertaining to mobile-bed equilibrium in the absence of seepage were accurately predicted using a sediment transport relation of the Meyer-Peter and Müller type. This notwithstanding, any test of the Shields number as a characterization of sediment mobility is best performed in terms of a sediment transport relation based on the Shields number. The data were used to develop such a relation where the exponent of 1.5 in the original Meyer-Peter and Müller formula was retained. The volume bed-load transport rate per unit width q_b was made dimensionless in terms of the Einstein number q_*, where

$$q_* = \frac{q_b}{\sqrt{\frac{\rho_s - \rho}{\rho} g D_{50} D_{50}}} \tag{23}$$

As illustrated in Fig. 5, the data were fitted to a sediment transport relation of the form

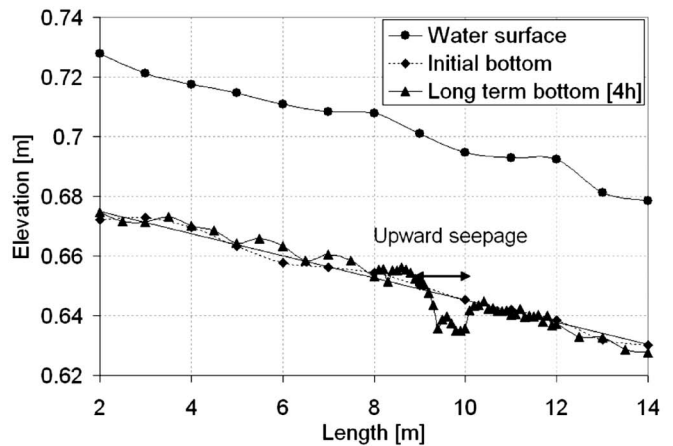$$q_* = 4.4158 \cdot (\tau_*' - \tau_{*cr})^{1.5} \tag{24}$$

where the critical Shields number τ_{*cr} takes the above-quoted value of 0.0332. Eq. (24) is similar to the corrected form of the bed-load transport equation of Meyer-Peter and Müller (1948) given in Wong and Parker (2006).
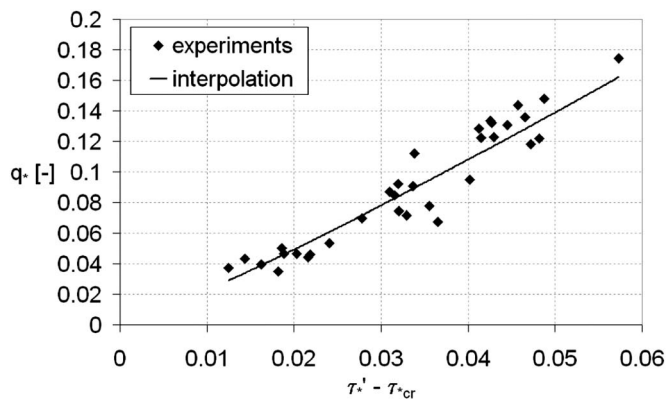
**Fig. 5.** Bed-load transport relationship, interpolated from experimental data
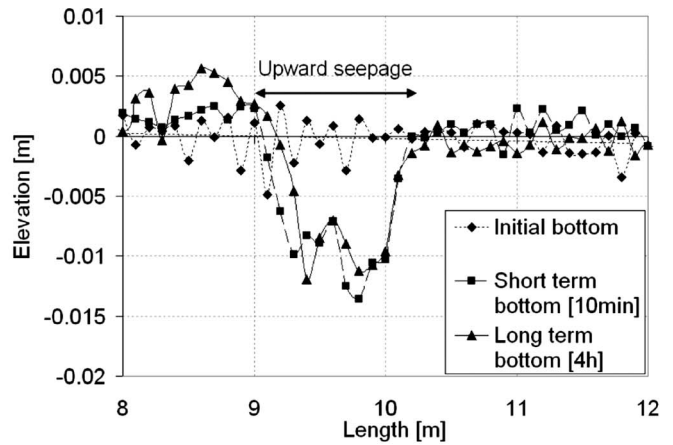
(a)

(b)

Fig. 6. Bed elevation profiles in case of upward seepage (Run 2-3, $Q_w = 16$ L/s, $Q_{seepage} = 60$ L/min). (a) Local scour bed due to upward seepage after the short-term experiment. The effect of average longitudinal slope has been subtracted; (b) equilibrium configuration due to upward seepage after the long-term experiment.

Experiments on Effect of Seepage on Bed Morphodynamics

The general experimental apparatus used for sediment recirculation has been described above for the experiments in the absence of seepage. This same system, which conserves the total amount of sediment in the system, was also employed for the experiments with seepage. The experiments with seepage were performed immediately after the experiments with no seepage. The experiments with no seepage were continued for a sufficiently long time to ensure that an equilibrium mobile-bed condition was achieved before commencing seepage. A total of 28 short-term experiments are reported here; only 25 long-term experiments are reported here because long-term experiments with a seepage flow of 140 L/min were not performed.

Fig. 6 illustrates the effect of upward seepage on bed morphology. The conditions are for those of Run 2-3, i.e., $Q_w = 20.6$ L/s and $Q_{seepage} = 60$ L/min. [A compendium of all measured bed profiles can be found in Francalanci, 2006; other examples of measured bed configurations are also reported in Francalanci et al., (2006).] Fig. 6(a) shows a view of the bed in the vicinity of the zone of seepage; the mean slope of the profile has been removed
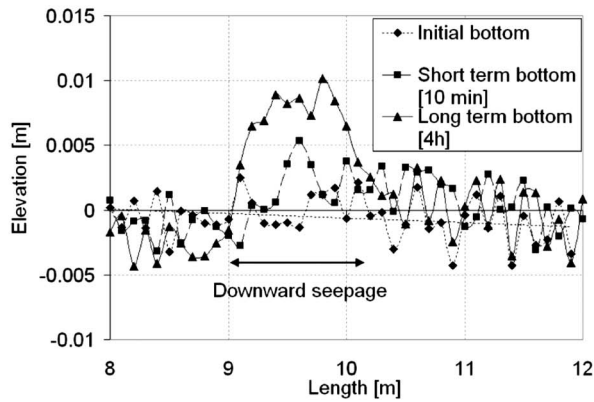
(a)
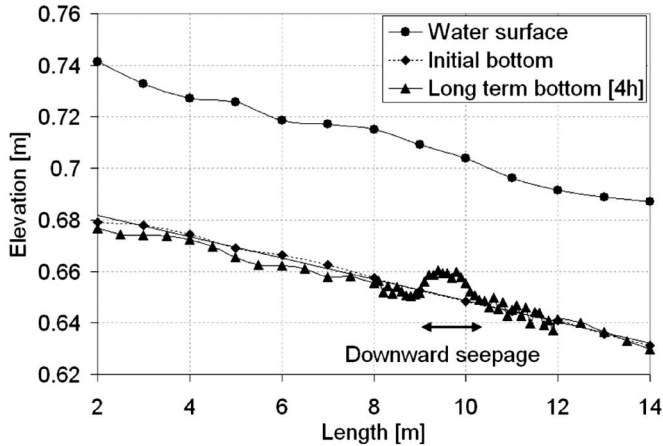
(b)

Fig. 7. Bed elevation profiles in case of downward seepage (Run 4-2, $Q_w=20.6$ L/s, $Q_{seepage}=60$ L/min). (a) Local scour bed due to downward seepage after the short-term experiment. The effect of average longitudinal slope has been subtracted; (b) equilibrium configuration due to downward seepage after the long-term experiment.

for clarity. The long profiles of the initial bed (i.e., bed at mobile-bed equilibrium in the absence of seepage), at the end of short-term experiment (10 min) and at the end of the long-term experiment (4 h) are shown. It is evident that the channel has scoured in the zone of seepage. Fig. 6(b) shows the initial and final long profiles of a much longer flume reach for the long-term experiment; the profiles have been detrended to remove the mean slope. Also shown in Fig. 6(b) is the water surface profile at the end of the long-term experiment. It is clear from Fig. 6(b) that scour in the seepage zone has been accompanied by some bed aggradation in the zone upstream. This pattern is dictated by the constraint of sediment recirculation; since the total mass of sediment is conserved, the mass of sediment eroded from the seepage zone must be deposited elsewhere.

Fig. 7 illustrates the effect of downward seepage. The conditions are those of Run 4.2, for which Q_w was equal to 20.6 L/s and $Q_{seepage}$ was equal to 60 L/min. Fig. 7(a) shows bed profiles for the initial condition (mobile-bed equilibrium in the absence of seepage), at the end of the short-term experiment (10 min) and at the end of the long-term experiment (4 h), all in the vicinity of the seepage zone. With regard to Fig. 6(a), the mean slope has been removed for clarity. The figure illustrates the effect of down-

ward seepage in inducing deposition. Fig. 7(b) shows the initial and final long profiles of a much longer flume reach for the long-term experiment; the profiles have been detrended to remove the mean slope. Also shown in Fig. 7(b) is the water surface profile at the end of the long-term experiment. With regard to Fig. 6(b), the deposition in the seepage zone has been accompanied by bed degradation upstream of the seepage zone.

Scour depth and thickness of deposition $\Delta\eta$ in the seepage zone were determined relative to the elevation of the bed at mobile-bed equilibrium before the onset of seepage. Two measures of scour were computed; the mean scour depth $\overline{\Delta\eta}$ and the maximum scour depth $\Delta\eta_m$. In the case of deposition these parameters take negative values. These quantities were made dimensionless into the respective forms $\bar{\varepsilon}$ and ε_m using the mean flow depth H that prevailed at mobile-bed equilibrium before the onset of seepage

$$\bar{\varepsilon} = \frac{\overline{\Delta\eta}}{H} \tag{25a}$$

$$\varepsilon_m = \frac{\Delta\eta_m}{H} \tag{25b}$$

Fig. 8(a) shows the dimensionless maximum scour/deposition depth ε_m as a function of the discharge ratio $Q_{seepage}/Q_w$; while in Fig. 8(b) the mean scour/deposition depths $\bar{\varepsilon}$ are shown versus $Q_{seepage}/Q_w$. Again, in both figures positive/negative values of ε_m and $\bar{\varepsilon}$ indicate scour/deposition, respectively.

The data are further stratified according to the Shields number τ_* prevailing at mobile-bed equilibrium before the onset of seepage, computed in accordance with Eqs. (17) and (21a). Data are shown in Figs. 8(a and b) for both the short-term experiments (open symbols) and long-term experiments (closed symbols). The overall tendency is for the magnitude of both measures of scour depth ε_m and $\bar{\varepsilon}$ to increase with increasing discharge ratio $Q_{seepage}/Q_w$. The long-term experiments show greater scour and deposition depths than the short-term experiments, indicating that 10 min is generally not sufficient to reach mobile-bed equilibrium in the presence of seepage. The data show only a weak tendency to stratify according to Shields number, with generally more scour at higher Shields numbers.

How Seepage Affects Bed Morphodynamics

The experimental results reported above clearly indicate that upward seepage induces scour and downward seepage induces deposition. Before pursuing a numerical model of the morphodynamics of erodible-bed open-channel flow in the presence of seepage, it is of value to provide an overview as to how flow-sediment interaction in the presence of seepage gives rise to scour or deposition. Three effects play important roles: (1) the effect of seepage on the bed shear stress τ_b; (2) the direct effect of seepage on the Shields number itself; and (3) the effect of seepage on the critical Shields number for the onset of motion.

Cheng and Chiew (1998a,b) have shown that over a wide range of conditions upward seepage reduces the bed shear stress τ_b in the zone of seepage. The same model implies that downward seepage increases the bed shear stress. The effect can be illustrated in terms of the St. Venant equations for conservation of water and flow momentum in the presence of seepage, which take the forms
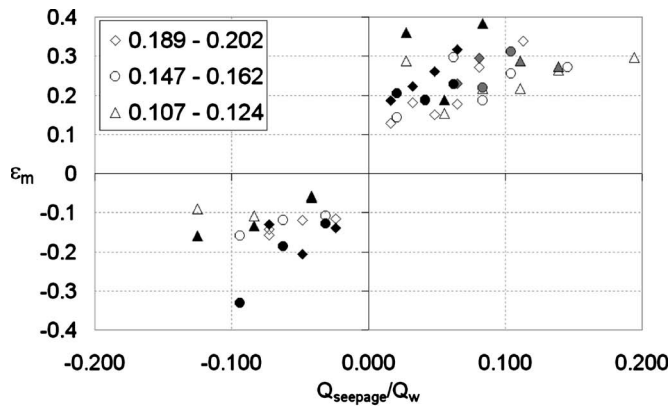
(a)
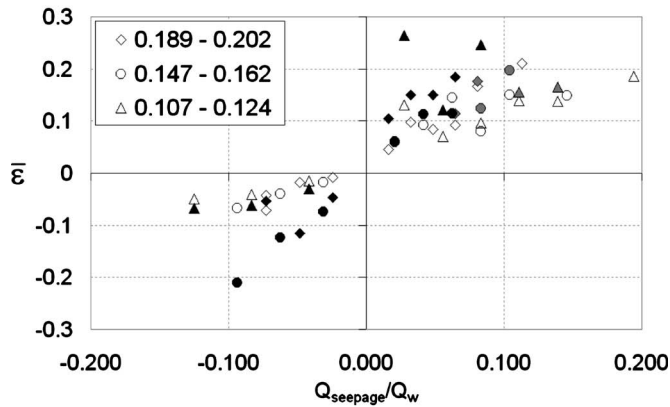
(b)

Fig. 8. Maximum and mean dimensionless scour and deposit depth plotted against discharge ratio $Q_{seepage}/Q_w$ for different range of average Shields parameter in case of zero seepage at equilibrium conditions, for short-term experiments (white dots—10 min) and for long-term experiments (black dots=4 h, gray dots=2 h). Note that positive values mean scour, negative values mean deposit. (a) Maximum dimensionless scour depth; (b) mean dimensionless scour depth.

$$\frac{\partial H}{\partial t} + \frac{\partial UH}{\partial x} = v_s \tag{26}$$

$$\frac{\partial UH}{\partial t} + \frac{\partial U^2 H}{\partial x} = -gH\frac{\partial H}{\partial x} + gHS - \frac{\tau_b}{\rho} \tag{27}$$

where x=streamwise distance; t=time; and U=depth-averaged flow velocity. Note that for simplicity the channel has been assumed wide enough to neglect sidewall effects in Eqs. (26) and (27). Reducing the above-two equations for steady flow, it is found that

$$\tau_b = \rho gHS - \rho gH\frac{dH}{dx}\left(1 - \frac{U^2}{gH}\right) - 2\rho Uv_s \tag{28}$$

The actual relation used by Cheng and Chiew (1998b) for bed shear stress is slightly different from Eq. (28) in that it allows for the velocity profile to be modified from the uniform flow by means of the momentum correction factor.

The first term on the right-hand side of Eq. (28) gives the standard depth-slope product rule for bed shear stress in the absence of backwater and seepage effects (and also the absence of sidewall effects). The third term on the right-hand side of Eq. (28)
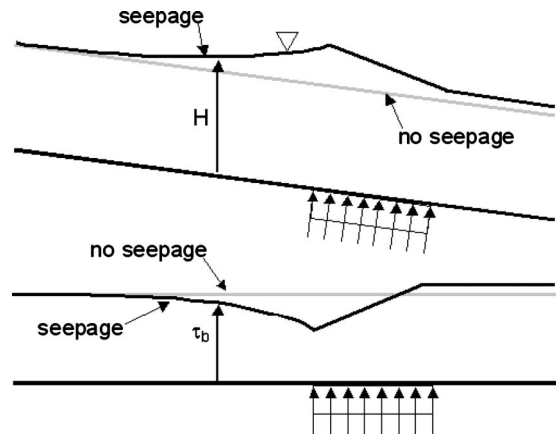
Fig. 9. Schematic diagrams showing patterns of flow depth H and bed shear stress τ_b induced by short zone of upward seepage. Profiles pertain to conditions before bed has evolved in response to seepage. Note that although bed shear stress in middle of seepage zone is below value prevailing in absence of seepage, it is above values prevailing in part of backwater zone immediately upstream of zone of seepage.

embodies the direct effect of seepage on bed shear stress; it invariably acts to decrease shear stress in the presence of upward seepage ($v_s > 0$) and increase it in the presence of downward seepage ($v_s < 0$). The second term in Eq. (28) embodies the effect of backwater generated by seepage. All the experiments reported here were verified to be such that the term $1 - U^2/(gH)$ was always positive in the seepage zone. In addition, dH/dx was negative in the seepage zone for upward seepage, and positive in the seepage zone for downward seepage. The second term in Eq. (28) thus always had a sign opposite to that of the third term in Eq. (28), but the magnitude was always less, and typically about one half. Thus the net effect of seepage was always to reduce the bed shear stress relative to the value that would prevail in the absence of seepage. This effect has been illustrated by Francalanci et al. (2005) and here it is briefly recalled. In particular, Fig. 8 of the aforementioned paper shows a plot of the ratio τ_b/τ_0 (ratio of the bed shear stress in the presence of seepage to the bed shear stress in the absence of seepage) versus the ratio $v_s/U_{upstream}$, with $U_{upstream}$ the flow velocity well upstream of the seepage region, and thus upstream of seepage-induced backwater. The results clearly indicate a suppression of bed shear stress in the presence of upward seepage. Also shown in the same figure are estimates obtained by Cheng and Chiew (1998b) for the case of upward seepage, which also illustrate the same trend. This finding is in qualitative agreement with the experimental results of Ali et al. (2003) on the effect of seepage on bed-load transport.

The effect of upward seepage, i.e., to reduce bed shear stress at the middle of the seepage zone relative to the value that would prevail in the absence of seepage, suggests that this effect alone would lead to deposition rather than scour in the zone of upward seepage. This finding is, for instance, consistent with the results of Ramakrishna Rao and Sitaram (1999) who found erosion (not deposition) in the case of downward seepage. This conclusion is, however, not correct in the case of the present experimental layout because it does not account for the entire profile of bed shear stress created by both the seepage and the backwater created by it. The profiles of flow depth H and bed shear stress τ_b prevailing immediately after the commencement of upward seepage over a short zone (but before the bed has had a chance to evolve mor-

phodynamically in response) are schematized in Fig. 9. Upward seepage creates a backwater effect upstream, such that H increases and bed shear stress τ_b decreases downstream toward the upstream end of the seepage zone. The effect of upward seepage on subcritical flow is such that the depth decreases, and the flow velocity and bed shear stress increase over the seepage zone. As a result the bed shear stress in the middle of the seepage zone is below the value prevailing in the absence of seepage, but above the bed shear stress in the backwater zone immediately upstream of the seepage zone. This pattern causes deposition in the backwater zone upstream of the zone of upward seepage, but scour in the seepage zone itself. The pattern is reversed in the case of downward seepage.

Two further effects of seepage act to change the mobility of the sediment itself. One of these is the direct effect of the seepage-induced nonhydrostatic pressure gradient on the denominator of the Shields number, as embodied in the forms Eqs. (12) and (16). The other of these is associated with a change in the critical Shields number τ_{*cr} in the presence of seepage, as elucidated by Cheng and Chiew (1999).

Darcy's law Eq. (14) can be rewritten in terms of the hydraulic gradient i as follows:

$$v_s = Ki, \quad i = -\frac{dh_p}{dz} = -\left(1 + \frac{1}{\rho g}\frac{dp}{dz}\right) \quad (29)$$

The critical upward seepage rate i_c at which the induced pressure force just balances the macroscopic weight of a granular bed, i.e., the bed becomes quick, is given by Cheng and Chiew (1999) as

$$i_c = \left(\frac{\rho_s}{\rho} - 1\right)(1 - \lambda_p) \quad (30)$$

where λ_p denotes bed porosity. As long as the hydraulic conductivity K remains independent of the seepage rate [a condition verified for the present experiments based on information in Cheng and Chiew, 1999], Eqs. (29) and (30) can be used to define a critical seepage rate v_{sc} for a quick bed such that

$$v_{sc} = K\left(\frac{\rho_s}{\rho} - 1\right)(1 - \lambda_p) \quad (31)$$

Now let $\tau_{*cr,s}$ denote the critical Shields number for the onset of sediment motion in the presence of seepage and $\tau_{*cr,a}$ denote the corresponding value in the absence of seepage. Cheng and Chiew (1999) find the following relation

$$\frac{\tau_{*cr,s}}{\tau_{*cr,a}} = 1 - \frac{v_s}{v_{sc}} \quad (32)$$

The above relation indicates that upward seepage decreases the threshold Shields number for the onset of sediment motion, as demonstrated by the experiments of Cheng and Chiew (1999) and recently confirmed by Dey and Zanke (2004). Conversely, downward seepage should increase the threshold Shields number for the onset of motion.

Numerical Model of Bed Morphodynamics in Presence of Seepage

The effect of seepage, and by extension nonhydrostatic pressure variation in the vertical direction near the bed, can be modeled numerically using a one-dimensional (1D) formulation. Where η denotes bed elevation, the Exner equation of sediment conservation takes the form

$$(1 - \lambda_p)\frac{\partial \eta}{\partial t} = -\frac{\partial q_b}{\partial x} \quad (33)$$

In a sediment-recirculating flume, the boundary condition on Eq. (33) is cyclic; i.e., where $x=0$ denotes the upstream end of the flume and $x=L$ denotes the downstream end

$$q_b|_{x=L} = q_b|_{x=0} \quad (34)$$

The bed shear stress in the numerical model was computed using a method that removes the effects of the vertical sidewalls, employing Eq. (19) given by Vanoni and Brooks (1957). In the experiments without seepage, the width-depth ratio B/H at mobile-bed equilibrium ranged from 10.0 to 15.7, values that are large enough to at least partially justify this approximation. The classical quasi-steady approximation was used in conjunction with the standard shallow water equations in calculating the flow, so that Eqs. (26) and (27) take the form

$$\frac{dUH}{dx} = v_s \quad (35a)$$

$$\frac{dU^2H}{dx} = -gH\frac{dH}{dx} + gHS - \frac{\tau_b}{\rho} \quad (35b)$$

Bed shear stress τ_b and the total and skin friction components of the dimensionless Chezy coefficient C and C', respectively, were evaluated as follows:

$$\tau_b = \alpha\rho\frac{U^2}{C^2} \quad (36a)$$

$$C = C' \cdot \sqrt{\frac{\tau'_*}{\tau_*}} \quad (36b)$$

$$C' = 8.10 \cdot \left(\frac{R'}{k_s}\right)^{1/6} \quad (36c)$$

with α being a correction coefficient ranging between 1.05 and 1.15, and with τ'_*/τ_* empirically determined from the correlation found in the case of mobile-bed experiments without seepage and expressed in Fig. 4. Note that the seepage can affect the distribution of the flow velocity, as outlined by Chen and Chiew (2004). As a first approximation this effect is not accounted for in the present numerical model. In the relation for C' [Eq. (36c)] due to Parker (1991), the roughness height k_s was computed as

$$k_s = n_k D_{90} \quad (37)$$

where the dimensionless parameter n_k was assumed to be about 2. Here the value of n_k was calibrated using experimental data for mobile-bed equilibrium flows in the absence of seepage, and the same value of n_k was applied to a corresponding experiment with seepage.

All the flows considered here were subcritical in the Froude sense. In the case of mobile-bed equilibrium without seepage, for example, the Froude number varied from 0.71 to 0.82. As a result, Eqs. (35a) and (35b) could be solved by integrating upstream from the downstream end of the flume. In principle the downstream boundary condition should consist of a set water surface elevation. The wall at the downstream end of the flume, however, imposed a set bed elevation instead. A quasi-equilibrium calculation using the backwater profile evaluated at the previous time step allowed an estimate of the downstream depth that: (1) led to the satisfaction of sediment conservation; and (2) speci-

fied a downstream boundary condition for a backwater calculation of the flow field which takes into account the constraint of non-erodibility of the bed near the overflow wall at the downstream end of the flume.

An abrupt change from a vanishing seepage velocity to a finite seepage velocity at $x=9$ m, and a similar abrupt change to vanishing seepage velocity at $x=10.1$ m tended to result in numerical instability in the model. Spurious oscillations were suppressed in two ways. First, an artificial diffusion term was added to Eq. (33), modifying it to

$$(1 - \lambda_p)\frac{\partial \eta}{\partial t} = -\frac{\partial q_b}{\partial x} + D_f \frac{\partial^2 \eta}{\partial x^2} \quad (38)$$

Values of D_f in the range $10^{-5} - 10^{-4}$ m^2/s were found to be adequate for this purpose. Second, the abrupt change in seepage velocity at the upstream and downstream ends of the seepage reach was replaced with very short zones over which seepage velocity varied smoothly according to a sinusoidal function. In addition, the seepage rate was slowly increased at the beginning of each numerical experiment until it attained its asymptotic value.

The effect of seepage was brought into the formulation in each of the three ways outlined in the previous section. The formulation of Eqs. (35a) and (35b) allows computation of the effect of seepage on the bed shear stress τ_b. In implementing the formulation of Eq. (24) for bed-load transport, the Shields number due to skin friction τ'_* was computed as

$$\tau'_* = \frac{\rho u'^2_*}{\left[\rho_s - \rho\left(1 + \dfrac{v_s}{K}\right)\right]gD_{50}} \quad (39)$$

using the generalization embodied in Eqs. (12) and (16) and τ_{*cr} was computed according to Eq. (32). Eq. (39) specifically brings the effect of a nonhydrostatic pressure distribution into the calculation of bed-load transport.

The equations were solved using an explicit finite-difference scheme, employing the predictor-corrector scheme, and upwinding in the computation of the spatial derivative of bed-load transport in Eq. (38). Results of the numerical calculations are presented in the next section.

Comparison of Experimental and Numerical Results

Comparisons of the results of the numerical model against those of the experiments for the case of upward seepage are given in Figs. 10(a and b). Both figures pertain to Run 1-3. Fig. 10(a) shows the initial measured bed profile (i.e., the profile at mobile-bed equilibrium in the absence of seepage), and the measured and computed final bed profiles at the end of the short-term experiment. Fig. 10(b) shows the corresponding profiles for the long-term experiment. Only a reach in the vicinity of the zone of seepage is shown in the figure; the effect of the mean bed slope has been removed from both figures for clarity. Figs. 10(a and b) show that the numerical model reasonably captures the observed pattern of seepage-induced scour both in the short and long terms. The numerically calculated profiles are smoother than the observed profiles because the numerical model does not capture the individual bed forms.

A similar comparison is shown in Figs. 11(a and b) for the case of downward seepage. Both figures pertain to Run 4-1, with the former figure characterizing the short term and the latter charac-
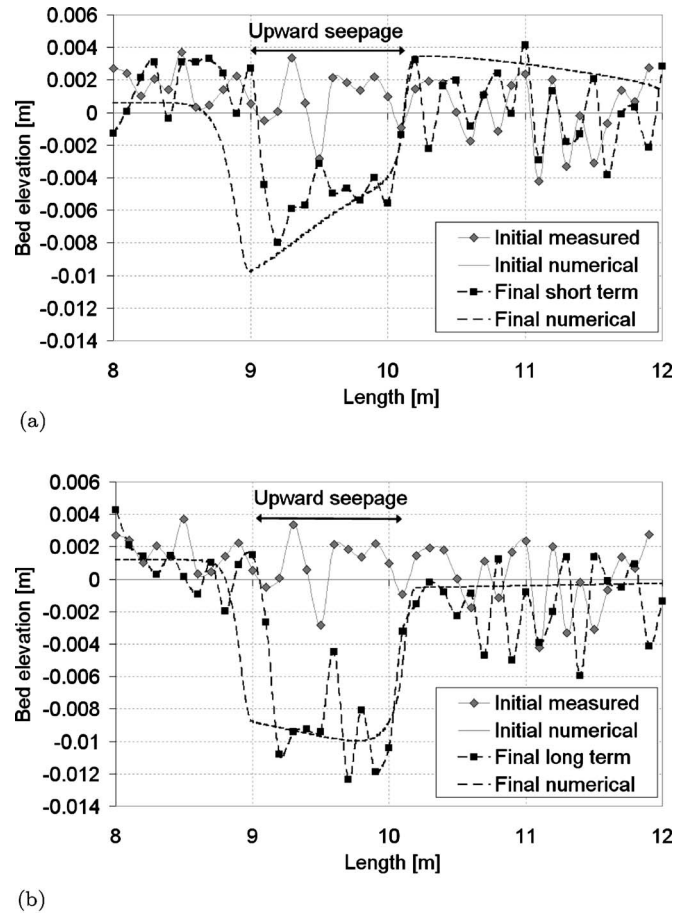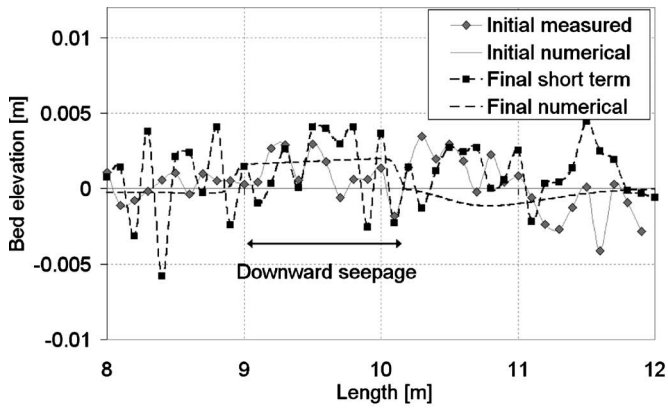

Fig. 10. Comparison of experimental and numerical results, Run 1-3: (a) short-term experiment; (b) long-term experiment

terizing the long term. The numerical model somewhat underpredicts the pattern of deposition induced by downward seepage, but the overall patterns of the experiments are clearly reflected in the model results.

It can be seen from Figs. 10 and 11 that the numerical model predicts that upward seepage increases the bed slope in the seepage zone as compared to mobile-bed equilibrium in the absence of seepage, and downward seepage similarly decreases the bed slope. Predictions in this regard are summarized in Figs. 12 for 15 runs with upward seepage and six runs with downward seepage. The results are for long-term calculations, with the bed slope computed as an average over the seepage zone.

Figs. 13(a and b) allow comparison between predicted and observed mean scour depth/deposition thicknesses. Similarly to Fig. 12, values are shown for 15 experiments with upward seepage and six experiments with downward seepage. Scour is represented in terms of the dimensionless parameter defined in Eq. (25a); the negative scour depths in Figs. 13(a and b) indicate deposition, the magnitude of the dimensionless thickness of which is given by Eq. (25a). Fig. 13(a) pertains to short-term experiments, and Fig. 13(b) pertains to long-term experiments. Dimensionless scour is plotted against the discharge ratio $Q_{seepage}/Q_w$.

The numerical model somewhat underpredicts the magnitude of both scour and deposition in the case of the lowest seepage flows, and slightly overpredicts the magnitude of both scour and deposition in the case of highest seepage flows. The trends are
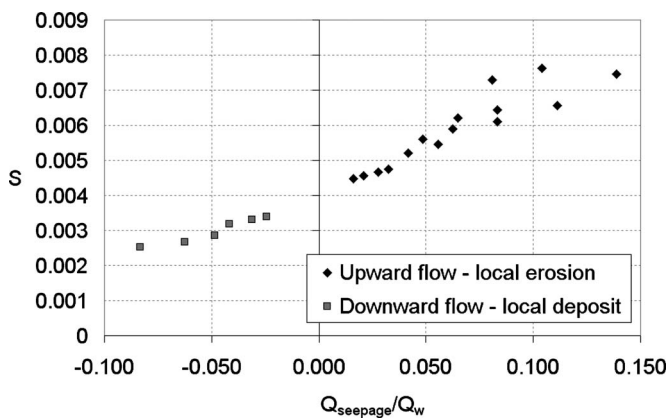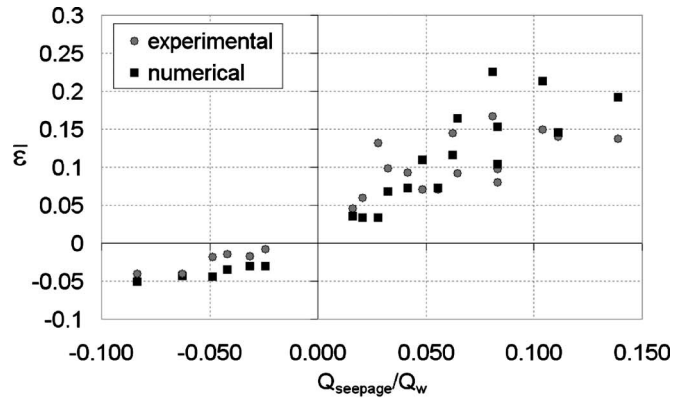
(a)
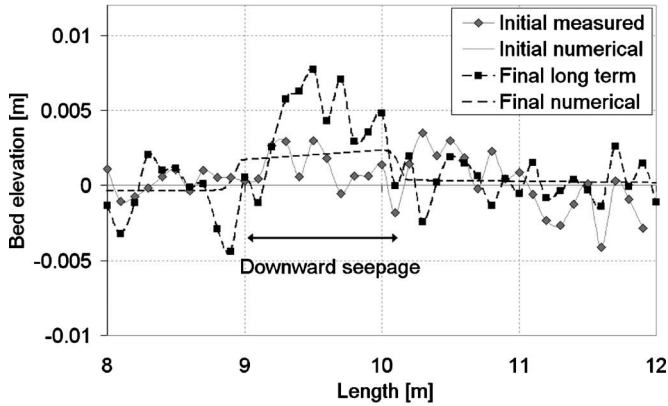
(b)

Fig. 11. Comparison of experimental and numerical results, Run 4-1: (a) short-term experiment; (b) long-term experiment

(a)

(b)

Fig. 13. Comparison of experimental and numerical results of mean scour in local seepage area. Positive values of mean scour indicate erosion, negative values indicate deposition. (a) Short-term experiment; (b) long-term experiment.
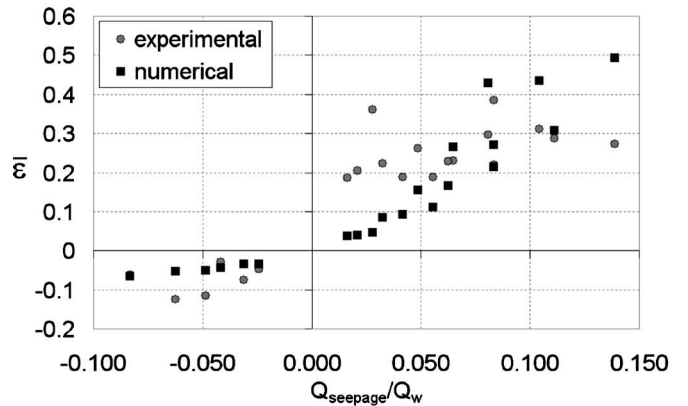
nevertheless very similar, and most of the predicted values fall within the scatter of the observed values. The results of Figs. 13(a and b) allow for the following tentative conclusion. Incorporation of the effect of seepage so as to (1) correct the prediction of the bed shear stress; (2) correct the critical Shields number; and (3) correct the expression for the Shields number itself so as to account for the nonhydrostatic vertical pressure gradient induced by seepage allows the numerical model to capture with reasonable accuracy the effect of seepage on bed mor-

Fig. 12. Average local slope, numerically computed, in upward/downward seepage area

phodynamics. It can similarly be tentatively concluded that the bed-load transport Eq. (24) determined in the absence of seepage effects can be applied to the case where a seepage-induced non-hydrostatic vertical pressure gradient prevails by means of the generalizations Eqs. (32) and (39).

Discussion

As noted above, the numerical model incorporates three modifications due to seepage: (1) modification of the bed shear stress τ_b; and modification of the parameters (2) τ'_*; and (3) τ_{*cr} used in the computation of bed-load transport. The effects of the nonhydrostatic pressure distribution induced by seepage are embodied in (2) and (3). It is of value to study the morphodynamic evolution that would result when factor (1) is retained but factors (2) and (3) associated with the nonhydrostatic pressure distribution are neglected. The predictions of the model in this case for bed evolution for a time duration of 1 h in the case of upward seepage only are shown in Fig. 14 (Run 1-2 HP, Run 1-5 HP), where the predicted bed profiles including all the nonhydrostatic pressure effects are also shown (Run 1-2 NHP, Run 1-5 NHP). The predicted patterns of scour and fill are very different from those obtained by including nonhydrostatic effects (see Francalanci et al. 2006, for analogous results for the case of short-term bed evolution). The implication is that the inclusion of nonhydrostatic
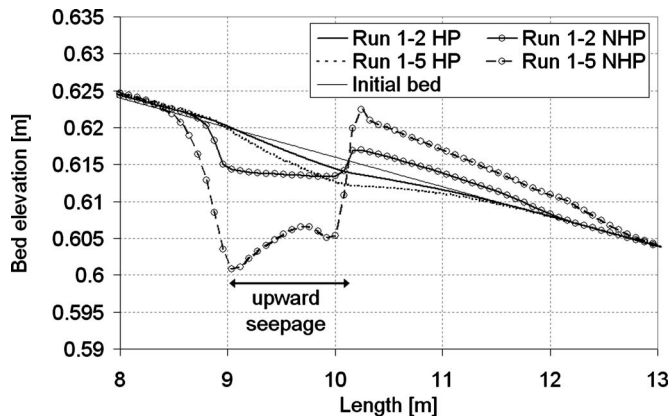
Fig. 14. Predictions of patterns of morphodynamic evolution in cases of (i) upward seepage when effect of seepage on bed shear stress is included, but effects of nonhydrostatic pressure gradient induced by seepage on bed-load transport are neglected (Run 1-2 HP, Run 1-5 HP); (ii) upward seepage including nonhydrostatic pressure effects (Run 1-2 NHP, Run 1-5 NHP)

effects is essential in order to obtain the generally good performance of the numerical model indicated by Figs. 13(a and b).

The generally positive performance of the numerical model as evidenced by Figs. 13(a and b) suggests the possibility of useful extensions to the computation of sediment transport in general nonhydrostatic flow fields. Examples of such flow fields are those which would prevail near an obstacle such as a bridge pier, abutment, or sharp river bend. Such flow fields should give rise to a near-bed gradient in the mean pressure field $\partial p / \partial x_i$ (averaged over turbulence) that deviates from hydrostatic in all three directions, rather than just the vertical direction considered here. The component of this pressure gradient vector, which acts tangential to the bed, generates a force that must be added to the impelling force associated with the tangential shear stress of the bed in computing sediment transport. The component of this pressure gradient vector acting normal to the bed exerts a force either pushing the particle against the bed (and so reducing mobility) or buoying it away from the bed (and so increasing mobility). A generalized formulation of sediment transport would naturally include all these effects, and so allow for an accurate computation of sediment transport in zones of highly nonhydrostatic pressure variation.

It is possible to predict the flow in more detail than is done here using a backwater formulation. More precisely, the Reynolds equations in combination with appropriate turbulence closure models such as k-ε and k-ω (Rodi 1980) as well as large-eddy simulation models predict not only the entire flow field but also the pressure field, including any deviation of the pressure (averaged over turbulence) from hydrostatic. Such models thus predict information that is as yet unused in the computation of sediment transport and scour near obstacles. The work presented here provides a first example as to how the predicted pressure field can be incorporated into calculations of sediment transport, and thus scour and fill near obstacles.

The real challenge in the computation of sediment transport and bed morphodynamics in the vicinity of obstacles as bridge piers is the accurate prediction of scour patterns. The flow field and bed topography near such obstacles is characterized not only by highly nonhydrostatic pressure fields, but also highly 2D patterns of boundary shear stress, as well as a bed that may have a substantial 2D bed slope. Parker et al. (2003), Francalanci (2006),

and Francalanci and Solari (2007) have developed tools to compute vectorial bed-load transport associated with vectorial bed shear stress and vectorial bed slope of substantial magnitude. The potential addition of the effect of nonhydrostatic pressure fields to the sediment transport formulation opens a new avenue toward the numerical evaluation of local scour via the linkage of higher-order fluid mechanical models of turbulent flow with higher-order nonlinear formulations for sediment transport.

One caveat deserves mention with regard to the effect of seepage on sediment transport. The general expression of the Shields number given by Eq. (16) is derived with the aid of Darcy's law Eq. (14) which is subject to some limitations in the case of a channel bed comprised of coarse sediments. In such a case, the seepage velocity is nonlinearly related to the pressure gradient. Moreover, the pressure force associated with vertical seepage given by Eq. (11) is accurate within a granular bed, but is subject to some inaccuracy at the boundary between the granular bed and the flow above. The accuracy of the model could be improved by means of a generalization to, e.g., the groundwater flow model of Brinkman (1947).

Conclusions

The dimensionless Shields number, or Shields stress, implicitly includes the assumption of a hydrostatic pressure distribution in its denominator. The assumption is reasonable for quasi-steady, quasi-uniform, rectilinear sediment transport, but breaks down in the case of sediment transport near an obstacle such as a bridge pier. A generalization of the Shields number is proposed for the case of a near-bed nonhydrostatic pressure gradient in the vertical direction. Such a gradient can be produced by upward or downward groundwater flow.

Experiments were performed in a water-feed, sediment-recirculating flume with a length of 15 m in order to study the effect of seepage on sediment transport. Experiments were performed in the absence of seepage to determine appropriate relations for flow resistance and sediment transport. Seepage was then induced over a 1.1 m reach toward the downstream end of a flume. Upward seepage caused scour in the zone of seepage; downward seepage produced deposition. These patterns were predicted reasonably well by a numerical model of morphodynamic evolution that incorporated the following seepage-induced effects: (1) modification of the bed shear stress; (2) modification of the critical Shields number for the onset of motion; and (3) modification of the Shields number itself to account for the nonhydrostatic pressure distribution.

The research suggests a new avenue toward the accurate prediction of sediment transport and scour patterns around flow obstacles such as bridge piers, where (1) the bed shear stress is strongly 2D; (2) the bed slope is strongly 2D and may be of substantial magnitude; and (3) the pressure distribution is strongly nonhydrostatic.

Acknowledgments

ence Foundation. This paper represents a contribution to the effort of NCED in the area of channel dynamics. Preliminary results of the present work were published in the Conference Proceedings of RCEM 2005 and River Flow 2006.

Notation

The following symbols are used in this paper:

B = channel width;
C_f = bed friction coefficient;
D = characteristic grain size of sediment at bed surface;
D_g = geometric mean size;
F_g = downward gravitational force;
F_g' = effective gravitational force;
F_p = Archimedian buoyant pressure force;
F_{pi} = vectorial pressure force acting on immersed grain;
g = gravitational acceleration;
H = flow depth;
h_p = piezometric head;
i = hydraulic gradient;
i_c = critical upward seepage rate;
K = hydraulic conductivity of granular bed;
Nh = dimensionless number to characterizing deviation from hydrostatic conditions;
p = pressure;
$Q_{seepage}$ = seepage discharge;
Q_w = inflow discharge;
q_b = volume bed-load transport rate per unit width;
q_* = dimensionless bed-load transport rate;
R = hydraulic radius;
S = equilibrium mean bed slope;
t = time;
U = depth-averaged flow velocity;
u_* = shear velocity;
u_*' = shear velocity of the bed region associated with skin friction
v_s = vertical velocity of seepage;
v_{sc} = critical seepage rate;
x_i = position vector in index notation;
$z = x_3$ = upward vertical coordinate;
$\Delta\eta$ = mean scour depth or thickness of deposition;
$\Delta\eta_m$ = maximum scour depth or thickness of deposition;
δ_{ij} = Kronecker delta;
$\bar{\varepsilon}$ = mean dimensionless scour depth or thickness of deposition;
ε_m = maximum dimensionless scour depth or thickness of deposition;
η = bed elevation;
λ_p = bed porosity;
ρ = density of water;
ρ_s = density of sediment;
σ_g = geometric standard deviation;
τ_* = dimensionless Shields number;
τ_b = boundary shear stress;
$\tau_c^*, \tau_{*cr,a}$ = critical dimensionless Shields number;
$\tau_{*cr,s}$ = critical Shields number for onset of sediment motion in presence of seepage;
τ_*' = dimensionless Shields number associated with skin friction; and
τ_*'' = dimensionless Shields number associated with form drag.

References

Ali, K. H. M., Achterberg, J., Li, M., and Zhu, Y. (2003). "Effect of seepage on sediment transport in channels." *Proc., Int. Conf. on Estuaries and Coasts*, IAHR, Hangzhou, China, 461–466.

Brinkman, H. C. (1947). "A calculation of the viscous force exerted by a flowing fluid on a dense swarm of particles." *Appl. Sci. Res., Sect. A*, 1, 27–34.

Chen, X., and Chiew, Y. M. (2004). "Velocity distribution of turbulent open-channel flow with bed suction." *J. Hydraul. Eng.*, 140(2), 140–148.

Cheng, N. S., and Chiew, Y. M. (1998a). "Modified logarithmic law for velocity distribution subjected to upward seepage." *J. Hydraul. Eng.*, 124(12), 1235–1241.

Cheng, N. S., and Chiew, Y. M. (1998b). "Turbulent open-channel flow with upward seepage." *J. Hydraul. Res.*, 36(3), 415–431.

Cheng, N. S., and Chiew, Y. M. (1999). "Incipient sediment motion with seepage." *J. Hydraul. Res.*, 37(5), 665–681.

Chien, N. (1954). "Meyer-Peter formula for bed-load transport and Einstein bed-load function." *M.R.D. sediment series, No. 7*, Univ. of California-Berkeley, and The Missouri River Division, U.S. Army Corps of Engineers, Berkeley, Calif.

Dey, S., and Zanke, C. E. (2004). "Sediment threshold with upward seepage." *J. Eng. Mech.*, 130(9), 1118–1123.

Francalanci, S. (2006). "Sediment transport processes and local scale effects on river morphodynamics." Ph.D. thesis, Univ. of Padova, Padova Italy.

Francalanci, S., Parker, G., and Paris, E. (2005). "Effects of non-hydrostatic pressure distribution on bedload transport." *Proc., Int. Symp. on River, Coastal and Estuarine Morphodynamics RCEM 2005*, G. Parker and M. H. Garcia, eds., Vol. 1, Taylor & Francis, London, 13–21.

Francalanci, S., Parker, G., and Solari, L. (2006). "Bedload transport in the case of seepage flow." *Proc., Int. Conf. on Fluvial Hydraulics River Flow 2006*, R. M. L. Ferreira, E. C. T. L. Alves, J. G. A. B. Leal, and A. H. Cardoso, eds., Vol. 2, Taylor & Francis, London, 1569–1576.

Francalanci, S., and Solari, L. (2007). "Gravitational effects on bed load transport at low Shields stress: Experimental observations." *Water Resour. Res.*, 43, W03424.

Meyer-Peter, E., and Müller, R. (1948). "Formulas for bed-load transport." *Proc., 2nd Meeting*, IAHR, Stockholm, Sweden, 39–64.

Parker, G. (1991). "Selective sorting and abrasion of river gravel. II: Applications." *J. Hydraul. Eng.*, 117(2), 150–171.

Parker, G., Seminara, G., and Solari, L. (2003). "Bedload at low Shields stress on arbitrarily sloping beds: Alternative entrainment formulation." *Water Resour. Res.*, 39(7), 1183.

Ramakrishnam, Rao A., and Sitaram, N. (1999). "Stability and mobility of sand-bed channels affected by seepage." *J. Irrig. Drain. Eng.*, 125(16), 370–379.

Rodi, W. (1980). *Turbulence models and their application in hydraulics—A state of the art review*, Institut fur Hydromechanik, University of Karlsruhe, Karlsruhe, Germany.

Seminara, G., Solari, L., and Parker, G. (2002). "Bed load at low Shields stress on arbitrarily sloping beds: Failure of the Begnold hypothesis." *Water Resour. Res.*, 38(11), 1249.

Shields, A. (1936). "Application of similitude mechanics and research on turbulence to bed load movement." *Mitteilungender Preussischer Versuchsanstalt fur Wasserbau und Schiffbau 26* (in German).

Vanoni, V. A., and Brooks, N. H. (1957). "Laboratory studies of the roughness and suspended load of streams," *Rep. No. E68*, Sedimentation Lab., California Institute of Technology, Pasadena, Calif.

Wong, M., and Parker, G. (2006). "Reanalysis and correction of bed-load relation of Meyer-Peter and Müller using their own database." *J. Hydraul. Eng.*, 132(11), 1159–1168.